Commun Nonlinear Sci Numer Simulat 131 (2024) 107841

Contents lists available at ScienceDirect

Communications in Nonlinear Science and Numerical Simulation

journal homepage: www.elsevier.com/locate/cnsns

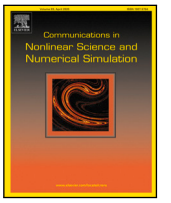

Research paper

Faraday kinks connecting parametric waves in magnetic wires

Alejandro O. Leon [a,*], Ernesto Berríos-Caro [b,c], Alejandra León [d], Marcel G. Clerc [e]

[a] Departamento de Física, Facultad de Ciencias Naturales, Matemática y del Medio Ambiente, Universidad Tecnológica Metropolitana, Las Palmeras 3360, Ñuñoa 780-0003, Santiago, Chile
[b] Department Theoretical Biology, Max Planck Institute for Evolutionary Biology, Plön, Germany
[c] Department of Evolutionary Ecology and Genetics, Christian-Albrechts-University of Kiel, Kiel, Germany
[d] Instituto de Ciencias Básicas, Facultad de Ingeniería y Ciencias, Universidad Diego Portales, Avda. Ejército 441, Santiago, Chile
[e] Departamento de Física and Millennium Institute for Research in Optics, Facultad de Ciencias Físicas y Matemáticas, Universidad de Chile, Casilla 487-3, Santiago, Chile

ARTICLE INFO

Keywords:
Topological Kinks
Faraday waves
Magnetic domain walls
Nonlinear magnetization dynamics
Parametrically driven systems

ABSTRACT

Kinks are domain walls connecting symmetric equilibria and emerge in several branches of science. Here, we report topological kinks connecting Faraday-type waves in a magnetic wire subject to dissipation and a parametric injection of energy. We name these structures *Faraday kinks*. The wire magnetization is excited by a time-dependent magnetic field and evolves according to the one-dimensional Landau–Lifshitz–Gilbert equation. In the case of high magnetic anisotropy and low energy injection and dissipation, this model is equivalent to a perturbative sine-Gordon equation, which exhibits 2π kinks that connect uniform states. We show that kinks connecting Faraday-type waves also exist in the damped and parametrically driven sine-Gordon equation, corresponding to the localized structures observed in the magnetic system. The solutions are robust; indeed, the bifurcation diagram reveals that kinks are stable, independently if the Faraday patterns are standing waves or have a dynamic amplitude or phase. Analysis of the nearly integrable limit of the sine-Gordon equation, as well as its description in terms of a fast and a slow variable, *i.e.,* the Kapitza limit, provide a useful interpretation of the kink as a non-parametric emitter that barely alters the fast standing waves. The existence of topological kinks connecting Faraday-type waves in the parametrically driven and damped Landau–Lifshitz–Gilbert and sine-Gordon equations, which model magnetic media, forced pendulum chains, and Josephson junctions, among other systems, suggest the universality of this self-organized structure.

1. Introduction

Localized states [1–4] are among the most common yet fascinating self-organized structures. In the simplest instance, localized states (LS) are particle-type solutions [4] that break the spatial translation symmetry. Their particle-type character allows characterizing them via their position, width, and velocity. Likewise, it motivates their use as information carriers in extended systems. One of the requisites of LS is a stable background [4] that can host one or several LS. However, the stability of the background implies that not all initial conditions will become localized states. Furthermore, the creation and control of LS can be a challenge in systems where the initial conditions are not well controlled, or fluctuations can destroy the LS in favor of the background equilibrium. Topological LS, however, are protected, becoming reliable information carriers. One of the most studied models exhibiting topological LS in one spatial dimension is the classical *sine-Gordon equation* (SGE) [5,6], which describes pendulum chains and Josephson junctions,

* Corresponding author.
E-mail address: aoleonv@utem.cl (A.O. Leon).

https://doi.org/10.1016/j.cnsns.2024.107841
Received 8 August 2023; Accepted 8 January 2024
Available online 12 January 2024

among several other systems. The solitons of the SGE are named kink and anti-kink and are domain walls connecting two physically equivalent states [5,7]. Therefore, various studies on topological LS focus on systems well described by the SGE in a specific limit. While the mapping is only exact in a small region of the parameter space, the LS inherited from the SGE kinks are usually robust in a broader set of parameters. Hence, one may expect the existence of topological kinks connecting more exotic solutions, such as *Faraday-type waves* [8], in generalized SGEs. These waves are nonlinear and emerge from spontaneous symmetry breaking in systems where a parameter that multiplies the state variable is time-modulated [9] and respond with a parametric resonance [10]. This driving mechanism induces several bifurcations when the forcing frequency is similar to twice the natural one, namely, in parametrically driven systems. Furthermore, experiments in vibrated granular media found a kink connecting two pattern domains with different oscillation phases [11–13]. Other systems with time-dependent forcing also display kinks [14–16].

At meso- and macroscopic scales, ferromagnetic systems are described by their magnetization. The temporal evolution of the magnetization is ruled by the Landau–Lifshitz–Gilbert equation [17]. At equilibrium, the magnetization points towards the net, or effective, magnetic field [17]. Since the magnetization norm is constant, uniform magnetization dynamics resemble pendulums orienting towards gravitational acceleration. Indeed, in the presence of a strong easy-plane magnetic anisotropy, the Landau–Lifshitz–Gilbert equation can be mapped to a generalized SGE [18], which models chains of planar pendulums. This limit has allowed several studies on localized magnetization structures [18–23]. Furthermore, at the onset of the parametric resonance, several LS emerge [24–32]. While the reduction to the sine-Gordon equation is exact only if the easy-plane anisotropy field is infinitely large, it is still an excellent qualitative, and several times quantitative, model for studying various magnetic systems. Indeed, the approximation of a phase space by an attractive manifold of smaller dimension displaying attractors with topological properties is a usual approach in physics. For example, the 2π kinks and anti-kinks of the SGE correspond to topological solitons in magnetic systems. Moreover, 2π kinks pump evanescent waves from its core when the magnet is subject to an oscillatory field [33]. Due to such wave emissions, kink–antikink bound states appear [33]. In two spatial dimensions, 2π kinks develop transverse instabilities, resulting in one-dimensional patterns along the domain wall [34]. While static and dynamic magnetic 2π kinks asymptotically connecting uniform states have been vastly studied, magnetic domain walls between more exotic equilibria have not been fully explored.

In this work, we report 2π kinks connecting Faraday-type waves, as shown in Fig. 1, in a parametrically driven, damped magnetic wire. Large anisotropy fields favor configurations where the unit magnetization vector lies on the plane perpendicular to the wire, and then the magnetization is parametrized by an angle ϕ. Spatial connections (fronts, or domain walls) between the equivalent states $\phi = 0$ and $\phi = 2\pi$ are stable and named 2π kinks. When the magnet is under the influence of a magnetic field with a static part and one that oscillates at twice the system's natural frequency, Faraday-type waves can emerge, as shown in Fig. 2. They are standing nonlinear waves that result from the instability of the $\phi = 0$ (or, equivalently, the $\phi = 2\pi$) equilibrium. We numerically show that kinks connecting patterns centered on the $\phi = 0$ and $\phi = 2\pi$ exist in a large zone of the parameter space. However, when the injection of energy surpasses a threshold, Faraday-type waves destroy the kinks. To verify the universality and structural robustness of our predictions, we study numerically and analytically the parametrically driven damped SGE and show the existence of the topological 2π kinks embedded in Faraday-type waves. Therefore, we expect these structures to emerge in several systems, ranging from mechanical resonators to superconducting junctions.

2. Parametrically driven magnetic wire

Let us consider a magnetic wire, where the unit magnetization field $\mathbf{m}(t, z)$ depends on time, t, and the spatial coordinate along the wire, z. A typical decomposition of $\mathbf{m}$ is along the Cartesian axes, $\mathbf{m} = m_x\mathbf{e}_x + m_y\mathbf{e}_y + m_z\mathbf{e}_z$, where $\mathbf{e}_j$ is the unit vector of the j-th Cartesian axis, see Fig. 1(a). The Landau–Lifshitz–Gilbert equation [17] governs the magnetization dynamics and, in its dimensionless form, it reads

$$\partial_t\mathbf{m} = -\mathbf{m}\times\mathbf{h}_{\text{eff}} + \alpha\mathbf{m}\times\partial_t\mathbf{m}, \tag{1}$$

where effective field is $\mathbf{h}_{\text{eff}} = h\mathbf{e}_x - \beta m_z\mathbf{e}_z + \partial_{zz}\mathbf{m}$. The first torque of Eq. (1) accounts for the counterclockwise precessions of $\mathbf{m}$ around the effective field $\mathbf{h}_{\text{eff}}$, and the term proportional to the damping constant α is the dissipation torque accounting for the energy losses. The effective field $\mathbf{h}_{\text{eff}}$ has three contributions: an external field $h\mathbf{e}_x$ pointing along the x axis, an anisotropy field proportional to β that favors magnetization motions in the x–y plane, and a dispersion term $\partial_{zz}\mathbf{m}$. The symbols ∂_t and ∂_z stand for temporal and spatial derivatives, respectively. The magnetic energy associated with the dispersion torque is proportional to $\int|\partial_z\mathbf{m}|^2dz$ and is minimized for uniform states. The norm conservation, $|\mathbf{m}| = 1$, motivates using the spherical representation,

$$\mathbf{m} = \sin(\theta)\left[\cos(\phi)\,\mathbf{e}_x + \sin(\phi)\,\mathbf{e}_y\right] + \cos(\theta)\,\mathbf{e}_z, \tag{2}$$

where θ and ϕ are the polar and azimuthal angles, respectively. The high anisotropy ($\beta \gg 1$) limit of Eq. (1) is [18]

$$\theta = \frac{\pi}{2} + \frac{\partial_t\phi}{\beta}, \tag{3}$$

$$\partial_{tt}\phi = -\bar{\omega}^2\sin(\phi) + \partial_{\zeta\zeta}\phi - \mu\partial_t\phi, \tag{4}$$

where $\bar{\omega} \equiv \sqrt{\beta h}$ is the angular frequency, $\zeta \equiv \beta^{-1/2}z$ is a renormalized space coordinate, and $\mu \equiv \alpha\beta$ is a damping constant. In Eqs. (3) and (4), we considered $\alpha \sim h \sim 1/\beta$, and only the dominant order terms in the small expansion parameter $1/\beta$ were admitted. In this limit, the polar angle θ is a slave variable that slightly deviates from the $\pi/2$ value, *i.e.,* most of the magnetization

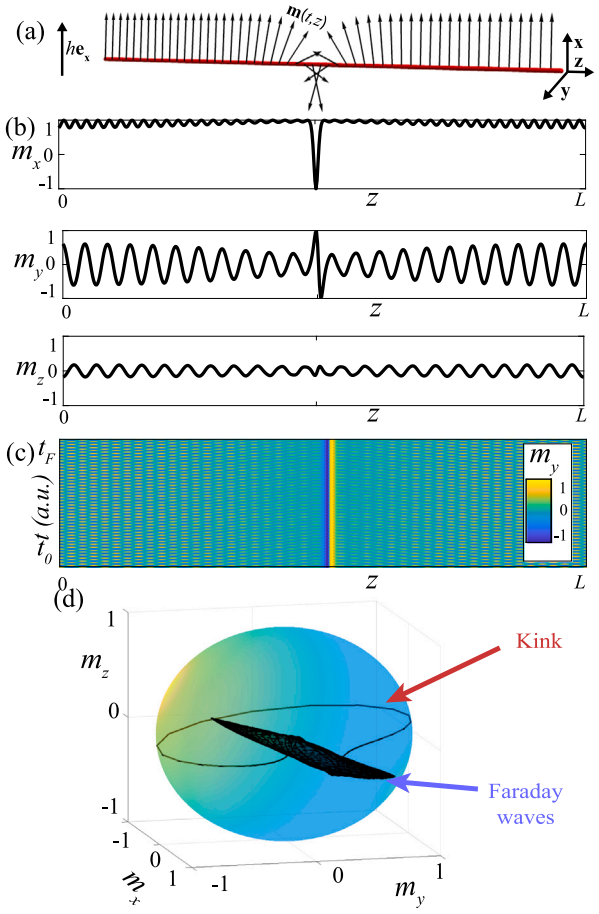

Fig. 1. Kink connecting Faraday-type waves. (a) Schematic representation of a magnetic wire, which is long in the z-axis and shorter in the other dimensions. The magnetization is uniform in the x and y coordinates and then it depends only of t and z, $\mathbf{m}(t,z)$. A large magnetic field along the x-axis polarizes the magnetization. The arrows depict the magnetization field for a Faraday kink. (b) Magnetization components m_x, m_y, and m_z as a function of the spacial coordinate $z \in [0, L]$ for a given time t_0. As this figure illustrates, the kink is a large structure that localizes between pattern domains. (c) Spatiotemporal diagram of $m_y(t,z)$ in the time interval $[t_0, t_F]$. The waves at the left and right of the kink oscillate with the same frequency, temporal phase, and wavenumber, while the kink position remains almost constant. (d) Magnetization field $\mathbf{m}$ parametrized by the position z at a given time. The magnetization lies on a unit sphere. While the Faraday-type waves are around the $m_x = 1$ point, the kink is a large loop-type excursion around the sphere. In the limit of infinite anisotropy, the magnetization lies on the (m_x, m_y) plane and the kink is a topologically protected structure. On the other hand, in this study, a finite anisotropy energy penalizes configurations with large m_z and, therefore, there is an energetic cost (finite nucleation barrier) involved in the creation and destruction of the kink.

lies in the x–y plane and therefore $|m_z| \ll 1$. Note that Eq. (4), which is a sine-Gordon equation (SGE) with dissipation, is invariant to 2π shifts. Therefore, the $\phi = 0$ and $\phi = 2\pi n$ solutions are symmetric for an integer n.

Another solution of Eq. (1) is $\mathbf{m} = -\mathbf{e_x}$, corresponding to a magnetization vector pointing opposite to the applied field. This unstable state is equivalent to the $\phi = \pi$ solution of the sine-Gordon equation, sometimes depicted as pendula pointing upwards, *i.e.,* against the gravitational acceleration vector. Fronts connecting the $\phi = 0$ (or $\phi = 2\pi$) and $\phi = \pi$ states are characterized by the invasion of the stable state over the unstable one. These domain walls are different from Faraday kinks because, in the case studied here, the kink connects the solutions $\phi = 0$ and $\phi = 2\pi$ that have identical properties, which results in a non-propagative wall.

Eqs. (1) and (4) display waves that decay to the $\mathbf{m} = \mathbf{e}_x$ and $\phi = 0$ equilibria, respectively. In order to induce permanent dynamics, we consider a time-dependent field, $h(t) = H_0 + h_0 \cos(\omega t)$, where H_0 and h_0 are the constant part and oscillation amplitude of h, respectively, and ω is the forcing angular frequency. In this case, one obtains the parametrically driven damped SGE,

$$\partial_{tt}\phi = -\left[\omega_0^2 + \gamma \cos(\omega t)\right] \sin(\phi) + \partial_{\zeta\zeta}\phi - \mu \partial_t \phi, \tag{5}$$

where $\omega_0 \equiv \sqrt{\beta H_0}$ is the natural angular frequency and $\gamma \equiv \beta h_0$ is the energy-injection parameter. The parametric resonance occurs for forcing frequencies near twice the natural one, namely, $\omega = 2(\omega_0 + \nu)$, where ν is a small detuning. In this regime, the dynamics of ϕ combine two scales: the fast oscillation with an angular frequency close to ω_0 and one from the slowly varying envelope. Furthermore, the oscillation amplitude evolves according to the parametrically driven damped nonlinear Schrödinger equation [15], which is obtained via weakly nonlinear analysis from the parametrically driven SGE and several models for other systems. This paradigmatic equation characterizes the emergence of Faraday-type waves [9]. These oscillatory patterns are observed

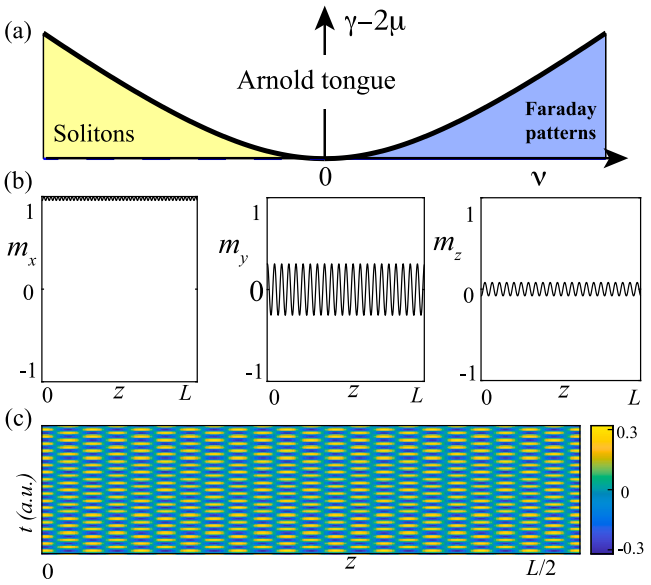

Fig. 2. Faraday-type magnetization waves emerging from the parametric instability of the uniform $\mathbf{m} = \mathbf{e}_x$ state. (a) Bifurcation diagram of a parametric resonance in the plane formed by the detuning, ν, and the energy injection with respect to the effective dissipation, $\gamma - 2\mu$. Inside the so-called Arnold tongue region, the $\phi = 0$ state (corresponding to $\mathbf{m} = \mathbf{e}_x$) is unstable, which gives rise to a diverse zoology [15]. At the left of the Arnold tongue, there are topologically trivial (or non-topological) solitary waves supported by the $\mathbf{m} = \mathbf{e}_x$ equilibrium. At the right of Arnold tongue, a spatial – also known as Turing or modulational – instability takes place and generates Faraday-type waves. These are the waves connected by the kink of Fig. 1. (b) Plots of m_x, m_y, and m_z as a function of z for a given time t_0. (c) Spatiotemporal diagram of Faraday-type patterns, these are waves with angular frequency and wavenumber approximately proportional ω_0 and $\sqrt{\nu}$, respectively.

for a positive detuning ($\nu > 0$) and when the energy injection overcomes a threshold, $\gamma \geq 2\mu$. The parametrically induced patterns grow with amplitude proportional to $\mu^{1/4}(\gamma - 2\mu)^{1/4} = \alpha^{1/4}\beta^{1/2}\left(h_0 - 2\alpha\right)^{1/4}$ and wavenumber $\nu^{1/2}$.

In the next subsection, we introduce our numerical methods, while Section 2.2 shows the characterization of the topological kink connecting Faraday-type patterns.

2.1. Numerical methods

Analytic studies of dynamic textures in non-autonomous nonlinear partial differential equations are limited to a few examples. Furthermore, in the present case, both the Faraday-type waves and the kink's core are large textures that make exact mathematical derivations an extremely difficult task. Therefore, we adopt a numeric approach to characterize our findings. The integration of the Landau–Lifshitz–Gilbert Eq. (1) is performed with a fifth-order Runge–Kutta algorithm for the temporal integration with a step size of $\Delta t = 3 \times 10^{-3}$. Stationary states are obtained after a transient time $t_0 \sim 10^4 - 10^5$, equivalent to $\sim 10^7$ iterations, which is long enough to reach the permanent dynamics, *i.e.,* the attractors of the system. The spatial discretization divides the wire into $N = 512$ segments of length $\Delta x = 0.3$. With sixth-order finite differences, the error of the Laplacian approximation is of order Δx^6. In the Cartesian representation, both periodic $\mathbf{m}(t, z+L) = \mathbf{m}(t, z)$ and Neumann $\partial_z \mathbf{m}(t, 0) = \partial_z \mathbf{m}(t, L) = 0$ boundary conditions yield similar results. The norm conservation, $|\mathbf{m}| = 1$, is monitored along the temporal integration. Dimensionless parameter values are $H_0 = 2$, $\beta = 10$, $\alpha = 0.02$, $\omega = 12$, and $0.385 \leq h_0 \leq 0.48$. The physical magnetic field ($B_{\text{ph},0}$), magnetization ($\mathbf{M}$), and space (z_{ph}) and time (t_{ph}) coordinates are obtained from their dimensionless counterparts via the following relations: $B_{\text{ph},0} = \mu_0 M_s h_0$, $\mathbf{M} = M_s \mathbf{m}$, $z_{\text{ph}} = l_{\text{ex}} z$, and $t_{\text{ph}} = \tau t$, where μ_0 is the magnetic permeability of free space, M_s is the saturation magnetization, l_{ex} is the exchange length, $\tau = \left(\gamma M_s\right)^{-1}$, and γ is the gyromagnetic ratio. For $CsNiF_3$, $M_s \approx 2.2 \times 10^5$ A/m, $l_{\text{ex}} = 5$ nm, and $\tau = 20$ ps [28].

2.2. Kinks: spatial connections between faraday-type waves

The magnetization depends on the angles ϕ and θ via trigonometric functions. Therefore, the magnetization and its dynamics remain unaltered when replacing ϕ with $\phi + 2n\pi$, n being an integer. Hence, if $\phi_0(t, z)$ is a solution, then $\phi_0(t, z) + 2n\pi$ is also a solution with the same properties. However, continuous connections between these symmetric equilibria are not necessarily stable. On the other hand, Fig. 1, obtained for $h_0 = 0.4$ and using periodic boundary conditions, demonstrates the existence of stable 2π kinks ($n = 1$) in this system, which are domain walls separating Faraday patterns centered around 0 and 2π.

The parameter space is explored using the continuation method, which integrates the system for a parameter value h_0 and uses the final magnetization as the initial condition for another parameter value, $h_0 + \Delta h_0$, with the small increment $\Delta h_0 = 10^{-3}$. Our results are summarized in Fig. 3. While kinks are observed for both periodic and Neumann boundary conditions, we employ the

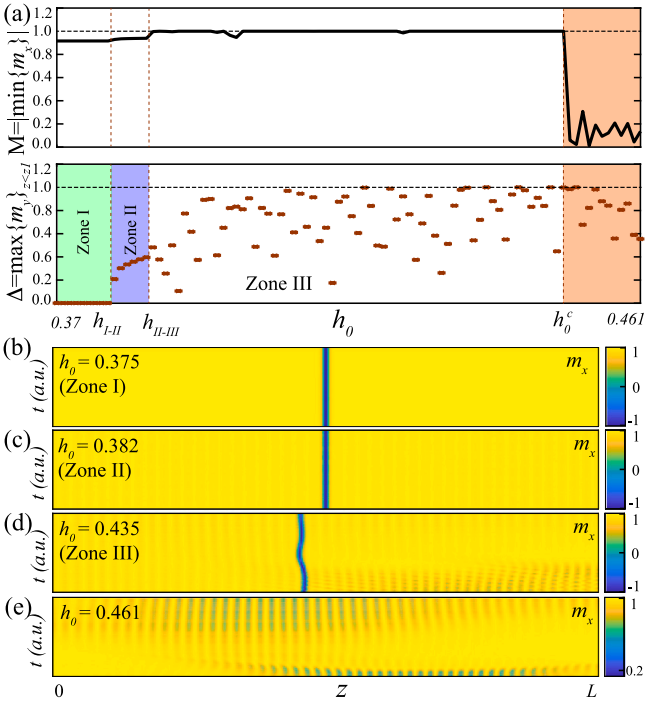

Fig. 3. Bifurcation diagram of Faraday kinks. (a) The dynamical indicator $M \approx 1$ when the kink is present and zero otherwise, *i.e.,* the topological charge of the texture is 1. M is defined as $M = \min\{m_1, m_2\}$, where $m_1 \equiv |\min\{m_x\}|$ and $m_2 \equiv 0.5(\max\{m_x\}\text{-}\min\{m_x\})$. The plot below considers the m_y deviations from the $m_y = 0$ value far from the kink core ($z_{\text{core}} \approx L/2$), $\Delta = \max\{m_y(t, z \le z_1)\}$. The M and Δ values allow identifying four regions. In Zone I, the kink exists ($M \approx 1$), and it asymptotically connects uniform states ($\Delta \approx 0$), as shown in spatiotemporal diagram (b). In Zone II, Faraday-type waves develop ($\Delta \not\approx 0$) at the left and right of the kink ($M \approx 1$), *c.f.* (c). Note that Δ grows monotonically in this region. In zone III, patterns develop instabilities due to the larger energy injection, which promotes their amplitude and phase to dynamical fields. In contrast with (b) and (c), spatiotemporal diagram (d) exemplifies that the core position moves for some h_0 values as a consequence of the patterns' phase dynamics. Finally, patterns are no longer stable for $h_0 \ge h_0^c = 0.449$, and only Faraday-type waves are observed. Other region borders are $h_{I-II} = 0.378$ and $h_{II-III} = 0.384$, and we use $z_1 = 25\Delta x = 7.5$.

latter for Fig. 3. When kinks are absent, m_x is similar to 1 due to the H_0 saturating field. However, since kinks are loops near the $m_z = 0$ plane in the **m**-space, the minimum of m_x approximates to -1. Therefore, a useful dynamical indicator is the absolute value of the minimum of m_x, $m_1 \equiv |\min\{m_x\}|$. However, m_1 does not distinguish between $m_x = 1$ and $m_x = -1$. To overcome this issue, we employ $M = \min\{m_1, m_2\}$, where $m_2 \equiv 0.5(\max\{m_x\}\text{-}\min\{m_x\})$. Fig. 3(a) shows that $M \approx 1$ in the vast region of the parameter space where the kink is stable. This indicator is qualitatively equivalent to assigning $M \to 1$, or topological charge 1, when the kink is present and 0 otherwise.

The region where the kink is stable is divided into three zones. First, in Zone I, where $h_0 \le h_{I-II} = 0.378$, the energy injection is insufficient for the spatial instability to develop, and the kink separates uniform states [33]. While the threshold for the emergence of Faraday-type patterns around the $\phi = 0$ uniform state is $h_0^{(0)} = 2\alpha$, the spatial instability of a kink requires a larger energy-injection threshold, *cf.*, Figs. 2 and 3. In the first region, $m_x \approx 1$ far from the core, as shown in the spatiotemporal diagram of Fig. 3(b), and therefore $m_y \approx 0$. This motivates the use of the maximum of m_y within a region $0 \le z \le z_1 = 7.5$, $\Delta = \max\{m_y(t, z \le z_1)\}$, as a second dynamical indicator. When $\Delta \approx 0$, there is no background texture far from the kink center.

In the second region, $h_{I-II} \le h_0 \le h_{II-III} = 0.384$, Faraday-type waves emerge. They are stationary patterns whose envelope is uniform and grows in a non-potential fashion. This is different from the expected 1/4 growth law of usual Faraday-type patterns [9]. Furthermore, the oscillation amplitude grows fast a function of the control parameter, exiting the weakly nonlinear regime. Consequently, the $\Delta \ll 1$ condition is fulfilled only within a tiny portion of the bifurcation diagram. Fig. 3(c) shows the spatiotemporal diagram of m_x in this zone. Note that the kink position is stationary. However, in the region of $h_{II-III} \le h_0 \le h_0^c = 0.449$, or zone III, Faraday-type waves develop several instabilities, which promotes the patterns' amplitude and phase to dynamic fields. Hence, the system exhibits kinks that connect states with irregular dynamics. A characteristic spatiotemporal diagram of this zone is illustrated in Fig. 3(d). The motions of the pattern drive the kink core and modify its shape, resulting in a moving LS. In zone III, the magnetization deviates considerably from 1, as revealed by $\Delta \lesssim 1$. After the threshold h_0^c, the kink disappears, as expected from the interaction with large amplitude patterns with dynamic phase and envelope. This is not surprising since the numerical integration of the system imposes a discretization that renders the topological protection to a significant, but finite, nucleation barrier. Additionally, the in-plane magnetic anisotropy is large, but also finite, and therefore the magnetization can exit the $m_z = 0$ plane if the energy injection is sufficient.

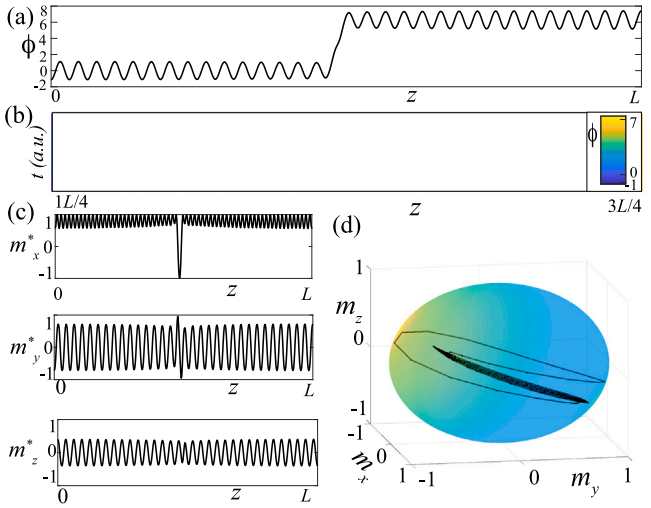

Fig. 4. Faraday kink in the parametrically driven damped SGE (5). (a) Profile of the field $\phi(x,t)$ at given time. The field ϕ shows patterns around $\phi = 0$ and $\phi = 2\pi$ at the left and right of the kink core, respectively. (b) Spatiotemporal diagram of ϕ. (c) Cartesian and (d) parametric plots of the magnetization reconstructed by mapping the fields ϕ and $\partial_t\phi$ that solve the SGE to $\mathbf{m}$ using Eqs. (2) and (3).

Note that we have studied the connections from 0 to 2π, but given the $z \to -z$ invariance of the magnetic wire, the solution jointing 2π and 0 exists and has the same properties reported here. An additional remark is that the h_{I-II}, h_{II-III}, and h_0^c reported here could change if a different initial condition (not the continuation method) is employed.

To verify the existence of the kink in other systems, the next section studies the parametrically driven damped SGE, which will also provide a more natural visual representation of the kink.

3. Parametrically driven damped sine-Gordon equation

The sine-Gordon equation models several systems [5,6], including classical scalar fields, superconducting junctions, and chains of weakly coupled pendulums. Therefore, the existence of a 2π kink connecting Faraday-type waves in this equation will allow us to hypothesize on the universality of this solution. Eq. (5) is integrated with the same parameter values and methods employed with the Landau–Lifshitz–Gilbert Eq. (1). The system can support topological charge 1 – corresponding to a single 2π kink – only if the generalized SGE is solved using Neumann boundary conditions, *i.e.*, $\partial_z\phi(t,0) = \partial_z\phi(t,L) = 0$. Figs. 4(a) and 4(b), obtained for $h_0 = 0.31$, show a characteristic kink snapshot and its spatiotemporal diagram. The patterns at the left and right of the kink are centered around the unstable states $\phi_{\text{left}} = 0$ and $\phi_{\text{right}} = 2\pi$, respectively. Using the fields $\phi(t,z)$ and $\partial_t\phi(t,z)$ that solve the generalized SGE (5), together with Eq. (2), we can reconstruct the magnetization field, which is shown as a function of the space, Fig. 4(c), and in the magnetization phase space, Fig. 4(d). As expected from the $\phi \to \phi + 2\pi$ invariance, the left and right waves map to the same magnetization pattern. However, the continuous connection between those waves crosses the $\phi = \pi$ point, where the magnetization approaches the $m_x = -1$ value. Then, the core of the SGE kink is mapped to a sizable localized magnetization structure.

The conservation of the magnetization norm restricts it to the unit sphere, $|\mathbf{m}| = 1$. In addition, the strong in-plane magnetic anisotropy favors magnetization configurations in the $m_z = 0$ plane. The combination of both constraints implies that the magnetization approximately lies on the $m_x^2 + m_y^2 = 1$ circumference and then is well-described by a single angle ϕ ruled by a generalized SGE. The Faraday-type waves are localized around the $m_x = 1$ point of the circumference, and kinks are complete 2π loops in this reduced phase space. The non-trivial topology of Faraday kinks originates on the geometry of this manifold with smaller dimensionality.

3.1. Perturbative analysis in the nearly integrable limit

Eq. (5) is integrable for $\gamma = \mu = 0$, which allows us to explore analytically the effect of small structural perturbations, such as finite dissipation and parametric injection of energy, on the 2π–kink solution. In this the nearly integrable limit, following [35–37], we write the parametrically driven damped SGE [see Eq. (5)] as:

$$\partial_{tt}\phi + \omega_0^2 \sin(\phi) - \partial_{\xi\xi}\phi = \epsilon P[\phi], \tag{6}$$

where $P[\phi] = -\gamma\cos(\omega t)\sin(\phi) - \mu\partial_t\phi$ denotes the perturbing terms and $\epsilon \ll 1$ is a small parameter. For the $\epsilon = 0$ case, this equation admits 2π–kink solutions of the form $\phi_{\text{SG}}(z) = 4\arctan\left[\exp(\sigma\, z)\right]$, where $z = \omega_0\gamma(v)(\zeta - \zeta_0 - vt)$, in which ζ_0 and v are the

central position and the speed of the kink's core, respectively, and $\gamma(v) = 1/\sqrt{1-v^2}$. The parameter σ takes the values $+1$ and -1, representing the kink and antikink solutions, respectively.

Based on inverse scattering transform approaches, one can derive analytical equations to describe the dynamics of the position ζ_0 and the speed v under small perturbations [35]. By promoting these parameters as time-dependent functions, one finds the following system of equations:

$$\frac{\mathrm{d}\zeta_0}{\mathrm{d}t} = -\frac{\epsilon\sigma}{4\omega_0^2} v(1-v^2) \int_{-\infty}^{+\infty} zP[\phi_{\mathrm{SG}}(z)]\,\mathrm{sech}\,(z)\,\mathrm{d}z, \tag{7}$$

$$\frac{\mathrm{d}v}{\mathrm{d}t} = -\frac{\epsilon\sigma}{4\omega_0} (1-v^2)^{3/2} \int_{-\infty}^{+\infty} P[\phi_{\mathrm{SG}}(z)]\,\mathrm{sech}\,(z)\,\mathrm{d}z, \tag{8}$$

which admits the following solutions

$$\frac{\mathrm{d}\zeta_0}{\mathrm{d}t} = \frac{\gamma\cos(\omega t)}{2\mu\omega_0^2}\frac{\mathrm{d}v}{\mathrm{d}t}, \tag{9}$$

$$v(t) = \sigma v_0 \frac{1}{\sqrt{v_0^2 + e^{2\epsilon\mu t}(1-v_0^2)}}, \tag{10}$$

where v_0 is the initial speed of the kink's core. These solutions demonstrate that the speed v of the kink's core gradually diminishes over time as a consequence of the dissipation, whereas the position ζ_0 experiences oscillations due to the action of the parametric forcing and tends to a steady value as time progresses. It is a matter of fact, the mobile wall becomes a stationary wall. These behaviors are consistent with the numerical simulation of the LLG and generalized sine-Gordon equations described in the previous sections.

While this perturbation analysis provides a good description of the dynamics of the kink's core in the nearly integrable limit, it is insufficient to provide a description of the observed Faraday-type waves. Consequently, the Faraday-type waves are far from the nearly integrable limit.

3.2. High-frequency limit

Following the strategy proposed by Kapitza [38], let us decompose the variable ϕ into its slow and a fast components, that is,

$$\phi(t,\zeta) = \phi_{\mathrm{slow}}(t,\zeta) + \phi_{\mathrm{fast}}(t,\zeta). \tag{11}$$

We assume that $\phi_{\mathrm{slow}}(t,\zeta) = \phi_{\mathrm{SG}}(t,\zeta)$, that is, that the slow variable is the $2\pi-$kink solution of the unperturbed sine-Gordon equation (see above). From now on, unless stated otherwise, we assume that $\sigma = 1$ and $v = 0$. In addition, we consider also that $|\phi_{\mathrm{fast}}(t)| \ll 1$ and that ϕ_{fast} evolves much faster than ϕ_{slow}, *i.e.*, $|\partial_t\phi_{\mathrm{fast}}| \gg |\partial_t\phi_{\mathrm{slow}}|$ and $|\partial_{tt}\phi_{\mathrm{fast}}| \gg |\partial_{tt}\phi_{\mathrm{slow}}|$.

Inserting the Ansatz from Eq. (11) into Eq. (5), and expanding in powers of the small ϕ_{fast} variable for a fast forcing frequency, we find

$$\begin{aligned}\partial_{tt}\phi_{\mathrm{fast}} = &-\gamma\cos(\omega t)\Big[\sin\left(\phi_{\mathrm{slow}}\right) + \phi_{\mathrm{fast}}\cos\left(\phi_{\mathrm{slow}}\right) \\ &- \frac{\phi_{\mathrm{fast}}^2}{2}\sin\left(\phi_{\mathrm{slow}}\right) - \frac{\phi_{\mathrm{fast}}^3}{6}\cos\left(\phi_{\mathrm{slow}}\right)\Big] + \partial_{\zeta\zeta}\phi_{\mathrm{fast}} - \mu\partial_t\phi_{\mathrm{fast}}.\end{aligned} \tag{12}$$

As this equation illustrates, the core of the kink plays the role of an oscillatory non-parametric injection of energy by the term $-\gamma\cos(\omega t)\sin\phi_{\mathrm{slow}}$. Far from the core, we have $\sin\phi_{\mathrm{slow}} = 0$ and ϕ_{fast} self-organizes into nonlinear standing waves to balance the injection and dissipation of energy. Numerical simulations of Eq. (12) show stationary pattern waves [see panels (a) and (b) in Fig. 5]. By combining this solution with ϕ_{slow}, we can reconstruct the Faraday kinks. Note that the expansion around ϕ_{fast} is of third power in order to ensure the standing-wave saturation far from the core. Eq. (12) can also serve as useful to describe the dynamics of evanescent waves observed in the flaming kinks reported in previous work [33].

4. Conclusions

Kinks are domain walls connecting symmetric states. While most studies concentrate on the interfaces between uniform states, kinks embedded in dynamic textures have received less attention. Here, we studied a kink connecting parametric or Faraday-type waves, or *Faraday kinks*, in a driven magnetic wire and in the sine-Gordon equation. Those standing waves are nonlinear patterns that can emerge when a system is forced at twice its natural frequency. Then, the kink divides the space between two regions of spatially and temporally periodic structures. The magnetization has a constant norm and then it lies on a spherical surface. If, in addition, the magnetic system has a large in-plane anisotropy, the magnetization will be restricted to a circumference. Then, a Faraday kink is a (2π radians) loop in this reduced phase space. Consequently, Faraday kinks are topologically protected while the in-plane anisotropy is dominant.

The Landau–Lifshitz–Gilbert equation rules the magnetization dynamics, and it can be mapped to a generalized sine-Gordon equation (SGE) for the azimuthal angle of the magnetization vector. The SGE reveals that the kink connects Faraday-type waves with their 2π shifted states (see Fig. 4). Using the nearly integrable limit of the SGE, we show that the kinks have a stationary core position due to the dissipation and the symmetry of the states that it connects. Additionally, in the fast oscillation limit, the

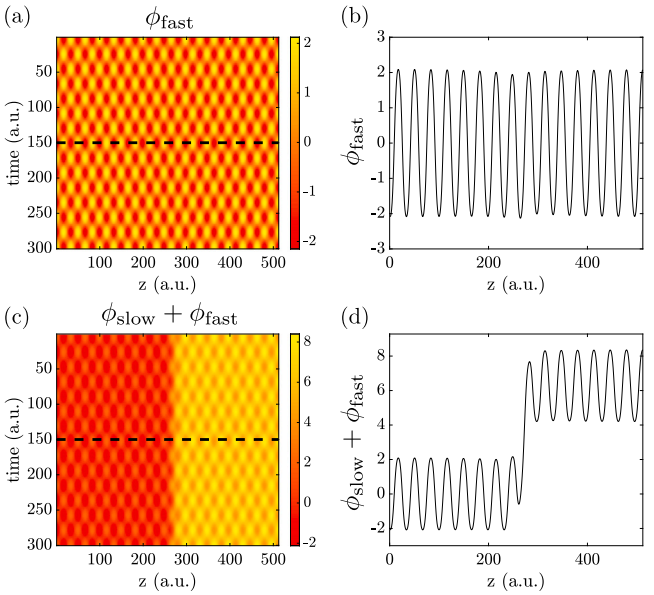

Fig. 5. Simulation outputs in the high-frequency limit. Panels (a) and (b) show the dynamics of the variable ϕ_{fast} described by Eq. (12), as a function of the spatial variable z (recall that $\zeta \equiv \beta^{-1/2} z$). The dashed line in panel (a) corresponds to the spatial profile shown in panel (b). Panels (c) and (d) show the same dynamics as in panels (a) and (b), but now adding the variable ϕ_{slow}. The slow variable ϕ_{slow} represents the $2\pi-$kink solution of the unperturbed sine-Gordon equation (*i.e.,* $\phi_{\text{slow}}(z) = 4 \arctan\left[\exp(z)\right]$). Parameters used: $H_0 = 2$, $\beta = 10$, $\alpha = 0.02$, $\omega = 12$, $h_0 = 0.40$, which translates into $\omega_0^2 = 20$, $\gamma = 4.0$, and $\mu = 0.2$.

application of a Kapitza-type method reveals that the kink core injects energy into the standing wave in a non-parametric fashion, becoming almost irrelevant for the fast-oscillating standing wave. The existence of kinks in the SGE allows one to conjecture their presence in the large variety of systems modeled by this equation, including Josephson junctions and coupled mechanical oscillators.

The bifurcation diagram of the magnetic kinks shows their persistence even if patterns become dynamic. When the injection of energy surpasses a value, kinks vanish.

Declaration of competing interest

The authors declare that they have no known competing financial interests or personal relationships that could have appeared to influence the work reported in this paper.

Data availability

Data will be made available on request.

Acknowledgments

We gratefully acknowledge financial support in Chile from FONDECYT, Chile Grant 11230120, 1211913, and 1210353; ANID-Millennium Science Initiative Program-ICN17-012 (MIRO). This research was supported by the Cluster Faraday UTEM, Chile (CONICYT- FONDEQUIP – EQM180180). EBC acknowledges the support of DFG, Germany through a Walter Benjamin Position grant, GZ: BE 8013/1-1, Projektnummer: 512851323.

References

[1] Cross MC, Hohenberg PC. Pattern formation outside of equilibrium. Rev Modern Phys 1993;65:851. http://dx.doi.org/10.1103/RevModPhys.65.851.
[2] Descalzi O, Clerc MG, Residori S, Assanto G, editors. Localized states in physics: solitons and patterns. Berlin Heidelberg: Springer Science & Business Media; 2011, http://dx.doi.org/10.1007/978-3-642-16549-8.
[3] Nicolis G, Prigogine I. Self-organization in nonequilibrium systems. New York: J.Wiley & Sons; 1977, http://dx.doi.org/10.1002/bbpc.197800155.
[4] Remoissenet M. Waves called solitons: concepts and experiments. Springer Science & Business Media; 2013, http://dx.doi.org/10.1007/978-3-662-03790-4.
[5] Scott A. Encyclopedia of nonlinear science. Routledge; 2006, http://dx.doi.org/10.4324/9780203647417.
[6] Cuevas-Maraver J, Kevrekidis PG, Williams F. The sine-Gordon model and its applications. New York: Springer; 2014.
[7] Pismen LM. Patterns and interfaces in dissipative dynamics. Berlin, Heidelberg: Springer; 2006, http://dx.doi.org/10.1007/3-540-30431-2.
[8] Faraday M. On a peculiar class of acoustical figures; and on certain forms assumed by groups of particles upon vibrating elastic surfaces. Philos Trans R Soc London 1831;121:299. http://dx.doi.org/10.1098/rstl.1831.0018.
[9] Coullet P, Frisch T, Sonnino G. Dispersion-induced patterns. Phys Rev E 1994;49:2087. http://dx.doi.org/10.1103/PhysRevE.49.2087.

[10] Landau LD, Lifshiftz EM. Mechanics, course of theoretical physics, vol. 1. New York: Pergamon; 1976, http://dx.doi.org/10.1016/C2009-0-25569-3.
[11] Denardo B, Wright W, Putterman S, Larraza A. Observation of a kink soliton on the surface of a liquid. Phys Rev Lett 1990;64:1518.
[12] Melo F, Umbanhowar PB, Swinney HL. Hexagons, kinks, and disorder in oscillated granular layers. Phys Rev Lett 1995;75:3838. http://dx.doi.org/10.1103/PhysRevLett.75.3838.
[13] Macías JE, Clerc MG, Falcón C, García-Ñustes MA. Spatially modulated kinks in shallow granular layers. Phys Rev E 2013;88. http://dx.doi.org/10.1103/PhysRevE.88.020201, 020201(R).
[14] Kityk AV, Knorr K, Müller H-W, Wagner C. Spatio-temporal Fourier analysis of Faraday surface wave patterns on a two-liquid interface. Europhys Lett 2004;65:857. http://dx.doi.org/10.1209/epl/i2003-10136-9.
[15] Clerc MG, Coulibaly S, Laroze D. Parametrically driven instability in quasi-reversal systems. Int J Bifurcation Chaos 2009;19:3525. http://dx.doi.org/10.1142/S0218127409024967.
[16] Goddard JD, Didwania AK. A fluid-like model of vibrated granular layers: Linear stability, kinks, and oscillons. Mech. Mater. 2009;41:637. http://dx.doi.org/10.1016/j.mechmat.2009.01.015.
[17] Mayergoyz ID, Bertotti G, Serpico C. Nonlinear magnetization dynamics in nanosystems. Oxford: Elsevier; 2009, http://dx.doi.org/10.1016/B978-0-08-044316-4.X0001-1.
[18] Mikeska HJ. Solitons in a one-dimensional magnet with an easy plane. J Phys C 1978;11. http://dx.doi.org/10.1088/0022-3719/11/1/007, L29.
[19] Kjems JK, Steiner M. Evidence for soliton modes in the one-dimensional ferromagnet $CsNiF_3$. Phys Rev Lett 1978;41:1137. http://dx.doi.org/10.1103/PhysRevLett.41.1137.
[20] Leung KM, Hone DW, Mills DL, Riseborough PS, Trullinger SE. Solitons in the linear-chain antiferromagnet. Phys Rev B 1980;21:4017. http://dx.doi.org/10.1103/PhysRevB.21.4017.
[21] Leung KM. Mechanical properties of double-sine-Gordon solitons and the application to anisotropic heisenberg ferromagnetic chains. Phys Rev B 1983;27:2877. http://dx.doi.org/10.1103/PhysRevB.27.2877.
[22] Zharnitsky V, Mitkov I, Levi M. Parametrically forced sine-Gordon equation and domain wall dynamics in ferromagnets. Phys Rev B 1998;57:5033. http://dx.doi.org/10.1103/PhysRevB.57.5033.
[23] Clerc MG, Coulibaly S, Laroze D. Localized states beyond the asymptotic parametrically driven amplitude equation. Phys Rev E 2008;77:056209. http://dx.doi.org/10.1103/PhysRevE.77.056209.
[24] Barashenkov IV, Bogdan MM, Korobov VI. Stability diagram of the phase-locked solitons in the parametrically driven, damped nonlinear Schrödinger equation. Europhys Lett 1991;15:113. http://dx.doi.org/10.1209/0295-5075/15/2/001.
[25] Clerc MG, Coulibaly S, Laroze D. Localized states and non-variational Ising–Bloch transition of a parametrically driven easy-plane ferromagnetic wire. Physica D 2010;239:72. http://dx.doi.org/10.1016/j.physd.2009.10.008.
[26] Clerc MG, Coulibaly S, Laroze D. Localized waves in a parametrically driven magnetic nanowire. Europhys Lett 2012;97:30006. http://dx.doi.org/10.1209/0295-5075/97/30006.
[27] Urzagasti D, Laroze D, Clerc MG, Coulibaly S, Pleiner H. Two-soliton precession state in a parametrically driven magnetic wire. J Appl Phys 2012;111. http://dx.doi.org/10.1063/1.3672872, 07D111.
[28] Urzagasti D, Laroze D, Clerc MG, Pleiner H. Breather soliton solutions in a parametrically driven magnetic wire. Europhys Lett 2013;104:40001. http://dx.doi.org/10.1209/0295-5075/104/40001.
[29] Clerc MG, Garcia-Ñustes MA, Zárate Y, Coulibaly S. Phase shielding soliton in parametrically driven systems. Phys Rev E 2013;87:052915. http://dx.doi.org/10.1103/PhysRevE.87.052915.
[30] Leon AO, Clerc MG. Spin-transfer-driven nano-oscillators are equivalent to parametric resonators. Phys Rev B 2015;91:014411. http://dx.doi.org/10.1103/PhysRevB.91.014411.
[31] Leon AO, Clerc MG, Coulibaly S. Traveling pulse on a periodic background in parametrically driven systems. Phys Rev E 2015;91:050901. http://dx.doi.org/10.1103/PhysRevE.91.050901.
[32] Leon AO, Clerc MG, Altbir D. Dissipative magnetic breathers induced by time-modulated voltages. Phys Rev E 2018;98:062213. http://dx.doi.org/10.1103/PhysRevE.98.062213.
[33] Berrios-Caro E, Clerc MG, Leon AO. Flaming 2π kinks in parametrically driven systems. Phys Rev E 2016;94:052217. http://dx.doi.org/10.1103/PhysRevE.94.052217.
[34] Berrios-Caro E, Clerc MG, Ferre MA, Leon AO. Oscillating decorated interfaces in parametrically driven systems. Phys Rev E 2018;97:012207. http://dx.doi.org/10.1103/PhysRevE.97.012207.
[35] Kivshar Yuri S, Malomed Boris A. Dynamics of solitons in nearly integrable systems. Rev Modern Phys 1989;61(4):763.
[36] McLaughlin David W, Scott Alwyn C. Perturbation analysis of fluxon dynamics. Phys Rev A 1978;18(4):1652.
[37] Tang Yi, Wang Wei. Perturbation theory for the kink of the sine-Gordon equation. Phys Rev E 2000;62(6):8842.
[38] Kapitza Pyotr Leonidovich. Dynamical stability of a pendulum when its point of suspension vibrates, and pendulum with a vibrating suspension. Collect Pap PL Kapitza 1965;2:714–37.